n-Dodecane hydroconversion over Ni/AlMCM-41 catalysts

Kegong Fang, Wei Wei, Jie Ren, and Yuhan Sun*

State Key Laboratory of Coal Conversion, Institute of Coal Chemistry, Chinese Academy of Sciences, Taiyuan 030001, P.R. China

Received 27 October 2003; accepted 16 January 2004

Mesoporous aluminosilicate (AlMCM-41) samples were synthesized using various aluminum sources: $Al(NO_3)_3$, aluminum isoproxide ($Al(OPr^i)_3$) and $NaAlO_2$. It was found that the AlMCM-41 prepared using $NaAlO_2$ contained more framework Al(IV) species and stronger acidity compared with those from $Al(NO_3)_3$ and $Al(OPr^i)_3$, respectively. Supported with 2.0 wt% nickel metal, the Lewis acid sites of the AlMCM-41 samples increased due to the compensating effect of the coordinately unsaturated nickel cations, while the Bronsted acid sites slightly decreased because of the coverage of the nickel species. In the *n*-dodecane hydroconversion, the Ni-containing AlMCM-41 sample prepared by using $NaAlO_2$ gave the symmetrical carbon number distribution and the largest amount of C_4–C_9 hydrocarbons in the cracked products due to its proper balance between metal and acid functions.

KEY WORDS: MCM-41; aluminum sources; *n*-dodecane; hydroconversion.

1. Introduction

The hydroconversion of *n*-paraffin is one of important processes in petroleum industry for obtaining good quality of middle distillates [1,2]. This process is usually carried out using a metal/acid bifunctional catalyst, over which the alkanes are dehydrogenated–hydrogenated on metallic sites and then isomerized or cracked on the acid sites through classical or nonclassical ion carbenium chemistry [3–5]. Thus, the balance between metal and acid sites is critical in determining the activity, stability and product selectivity of these catalysts [6–8].

In the past few decades, many studies have been performed on the catalytic performance of metal-loaded zeolite bifunctional catalysts. It was generally considered that microporous zeolite-based catalyst have advantages in producing lower coking and higher hydrocracking activity with respect to the amorphous catalysts [9]. However, their applications were limited in the conversion of large molecules due to the small pore size channel of microporous zeolites [10]. The Al-containing mesoporous MCM-41 materials possessing high surface area and tunable uniform mesopores have been considered as attractive model catalyst for the hydroconversion of normal paraffins [11]. Del Rossi and Chaudhari *et al*. reported that the Pt-supported on AlMCM-41 catalysts exhibited high isomerization selectivity in the hydroconversion of *n*-hexane [12,13]. Elangovan *et al*. studied the isomerization and hydrocracking of *n*-decane over Pt-Pd/AlMCM-41 catalyst and achieved higher catalytic activity than that of the monometallic Pt and Pd catalysts [11]. Klemt *et al*. reported that the NiMo/MCM-41 catalyst gave lots of hydrogenolysis products in the hydrocracking of *n*-decane and the methane generation could be reduced as the template in the mesostructure of AlMCM-41 was extracted by a NH_4NO_3 ethanol solution [14]. However, the catalytic performances of nickel-supported on Al-MCM-41 catalysts have not been studied yet in the hydroconversion of long-chain paraffins.

In the present study, several AlMCM-41 samples prepared with different aluminum sources were used as supports of nickel catalysts and their effects on the catalytic performance for the *n*-dodecane hydroconversion were investigated. The Ni-containing AlMCM-41 catalyst prepared by using $NaAlO_2$ was found to be a promising bifunctional catalyst for the hydrocracking–hydroisomerization of *n*-dodecane, which displayed a symmetrical carbon number distribution and the largest amount of C_4–C_9 hydrocarbons in the cracked products due to its proper metal/acid ratio.

2. Experimental

2.1. Catalyst preparation

Mesoporous AlMCM-41 supports were prepared hydrothermally using a gel mixture with the following molar composition:$1.0SiO_2$:$0.41Na_2O$:$0.033Al_2O_3$:0.2CTAB:$80H_2O$. Aluminum compound ($NaAlO_2$, $Al(NO_3)_3$ or $Al(OPr^i)_3$) was first dissolved in demineralised water and mixed with a certain amount of water glass. Then the cetyltrimethylammonium bromide (CTAB) aqueous solution was added to the above mixture with stirring. Subsequently, the pH of the gel mixture was adjusted to ca. 10.3 by dropwise addition of 2 M HCl. The resulting gel was transferred to a teflon-

* To whom correspondence should be addressed.
E-mail: yhsun@sxicc.ac.cn

1011-372X/04/0300–0235/0 © 2004 Plenum Publishing Corporation

lined autoclave and aged at 393 K for 48 h. The solid product recovered by filtration was washed with deionized water, dried in air at 333 K, and calcined at 873 K for 5 h to get the template-free AlMCM-41. The protonated form of AlMCM-41 was obtained by ion exchange with 1 M NH_4NO_3 solution twice at 323 K for 8 h, dried at ambient temperature, and then calcined at 813 K for 3 h.

The nickel-supported catalysts were prepared by the incipient wetness impregnation technique. Nickel was loaded on the support with proper amount of $Ni(NO_3)_2$ aqueous solution to get the 2.0 wt% Ni loading. After impregnation, the catalysts were dried at 393 K for 5 h and calcined at 673 K for 4 h in air.

2.2. Characterization

The Si/Al molar ratio of the calcined AlMCM-41 samples was determined by AES-ICP analysis. X-ray power (XRD) measurement was carried out using a Philips PW 1050/25 diffractometer with CuK_α radiation (50 kV, 30 mA). The textural properties of the samples were determined in a Micromeritics ASAP-2000 automated nitrogen physisorption apparatus. ^{27}AlMAS NMR spectra were recorded using a Bruker MSL-300 spectrometer. External $Al(H_2O)_6^{3+}$ was used as reference.

Ammonia temperature-programmed desorption (NH_3-TPD) was measured by a flow system with a thermal conductivity detector. All the catalysts (150 mg) were outgassed in argon flow at 873 K for 30 min, which followed ammonia-saturation by flowing NH_3/Ar stream at 373 K for 15 min. After equilibration in argon flow for 2 h at 373 K, the catalyst was heated in a linear rate of 10 K/min to 873 K, and the detector signal of ammonia desorption was recorded.

FT-IR spectra of adsorbed pyridine were recorded on a Nicolet Magna 550 Fourier transform infrared spectrometer at 4 cm^{-1} resolution. The sample was finely grounded and pressed into self-supporting wafer (10 mg/cm^2, diameter = 15 mm), and then placed into the measurement cell with CaF_2 windows. The evacuation at 773 K (ca. 10^{-4} Torr) for 4 h was carried out prior to adsorption of pyridine. IR spectra were recorded after subsequent evacuation at 433 K.

The temperature-programmed reduction (TPR) of the samples was performed in a flow system with a thermal conductivity detector. The samples (100 mg) were first outgassed in argon by heating to 773 K and then cooled at ambient temperature. Next, they were heated in an H_2/Ar (5/95 volumetric ratio) reducing gas mixture from room temperature to 1023 K by a heating rate of 10 K/min and the detector signal was recorded continuously.

Nickel dispersion was measured by H_2 chemisorption in a Pulse Chemisorb 2700 micrometrics. The samples were preheated at 723 K for 2 h in H_2 flow, followed by cleaning with Ar flow at 723 K for 30 min. Then the chemisorption experiments were performed at room temperature.

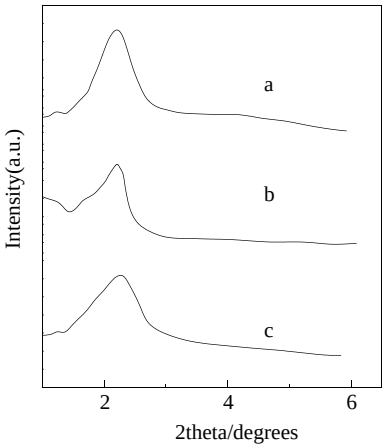

Figure 1. Powder XRD patterns of the samples. (a) AlMCM-41(A); (b): AlMCM-41(P); (c): AlMCM-41(N).

2.3. Catalytic test

n-Dodecane hydroconversion was carried out in a down flow fixed-bed stainless steel tube reactor (i.d. = 6 mm; 120 cm in length) at 2.0 MPa and H_2/*n*-dodecane molar ratio of 20. The catalyst was pretreated in Ar flow and then reduced *in situ* in a flow of H_2 at 723 K for 4 h prior to the start of the reaction. The gas products were analyzed by gas chromatograph with a GDX-103 column and FID detector, an ov-101 capillary column and FID detector for the liquid ones.

3. Results and discussion

3.1. Textural and phase structure

Figure 1 showed the XRD patterns of the calcined AlMCM-41 samples prepared with different aluminum sources. All the samples showed the major (100) peak, characteristic of the hexagonal order of the parent MCM-41 [15]. The intensity of the (100) peak in the case of AlMCM-41(A) was stronger than that of AlMCM-41(N) and AlMCM-41(P), indicating that the sample prepared with $NaAlO_2$ was more crystalline compared to those prepared with $Al(OPr^i)_3$ and $Al(NO_3)_3$.

The ^{27}Al MAS NMR spectra (see figure 2) illustrated that the three samples showed an intense signal at 52 ppm from 4-coordinate aluminum and a low-intensity signal at 0 ppm from 6-coordinate aluminum [16]. The relative intensities of the framework 4-coordinate aluminum increased in the order of AlMCM-41(N) < AlMCM-41(P) < AlMCM-41(A), contrarily to that of the 6-coordinate aluminum. The actual Si/Al ratio of AlMCM-41(A) determined by AES-ICP was more closer to that of the primary gel (see table 1). These implied that the aluminum atoms was more

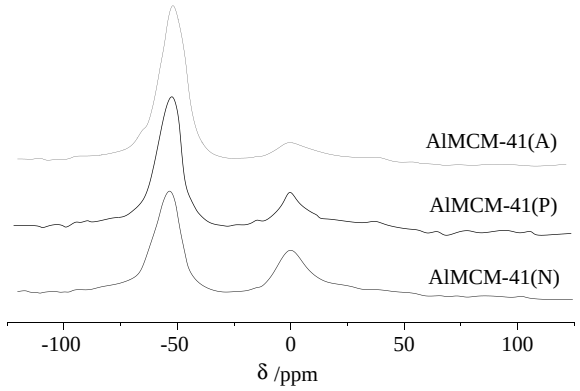

Figure 2. ^{27}Al MAS NMR spectra of calcined AlMCM-41 samples.

readily incorporated in the framework of MCM-41 prepared with $NaAlO_2$ than those from $Al(OPr^i)_3$ and $Al(NO_3)_3$.

The textural properties of the AlMCM-41 samples and their corresponding nickel-supported catalysts were given in table 1. The surface area, pore volume and average pore diameter of AlMCM-41(A) was higher than those of AlMCM-41(N) and AlMCM-41(P). After nickel impregnation, the surface area and the pore volume of the samples clearly decreased, suggesting that a partial collapse of the mesostructure took place due to the metal-support interaction and the hydrothermal treatment during the post-treatment of the catalysts [17–19].

3.2. Acidity

NH_3-TPD showed the acid strength of the AlMCM-41 samples was rather moderate, almost weak and medium acidity, and the total acid numbers decreased in the order of AlMCM-41(A) > AlMCM-41(P) > AlMCM-41(N) (see figure 3). This was consistent with the amount of framework Al(IV) in the samples, indicating that the acidity mainly resulted from 4-coordinate aluminum. Upon loaded with nickel, the catalysts had the same acid features as the corresponding AlMCM-41 supports. However, the total acid number of the Ni-containing samples was slightly more than that of their parent supports (see table 2), similarly to the behavior of Ni-modified Y zeolites [20]. This probably originated from the Lewis acid nature of nickel cations, which had been reported to have capability of retaining ammonia [21,22].

The Py-IR spectra and the acid distribution of AlMCM-41 and Ni/AlMCM-41 catalysts were shown in figure 4 and table 2. The Bronsted acidity appeared highest in AlMCM-41(A) and lowest in AlMCM-41(N). Considering that the tetrahedral aluminum atoms on the wall surface were more accessible to the basic probe

Table 1
Physicochemical properties of the Ni-supported catalysts

Catalysts	Al source	Si/Al ratio		S_{BET} (m^2/g)	Pore volume (cm^3/g)	Average pore diameter (Å)
		Gel	Crystal			
AlMCM-41(A)	$NaAlO_2$	15	15.8	895.3	0.85	36.7
Ni/AlMCM-41(A)	–	–	–	847.6	0.77	36.2
AlMCM-41(P)	$Al(OPr^i)_3$	15	16.7	700.1	0.61	33.5
Ni/AlMCM-41(P)	–	–	–	644.0	0.53	32.9
AlMCM-41(N)	$Al(NO_3)_3$	15	19.1	674.2	0.62	34.3
Ni/AlMCM-41(N)	–	–	–	618.7	0.52	33.7

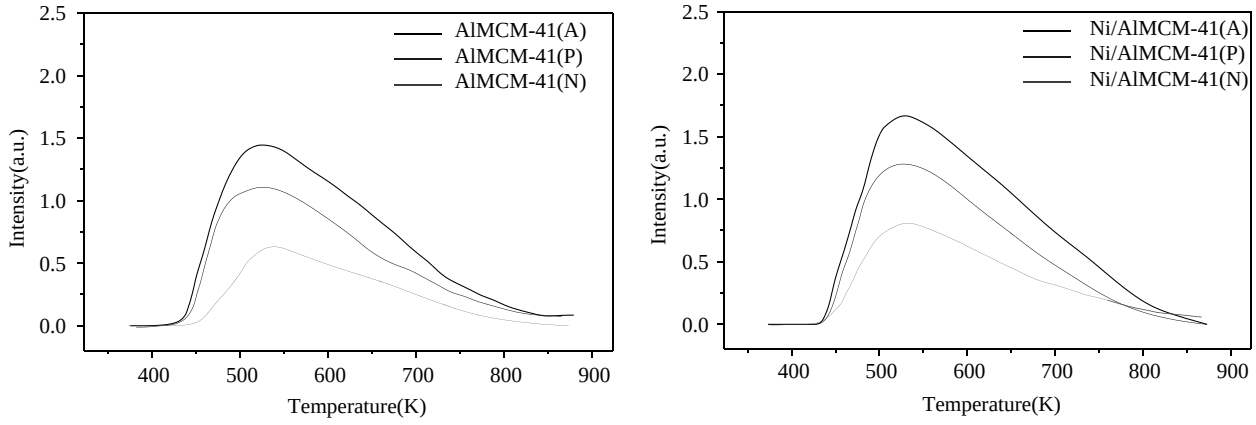

Figure 3. NH_3-TPD patterns of the catalysts.

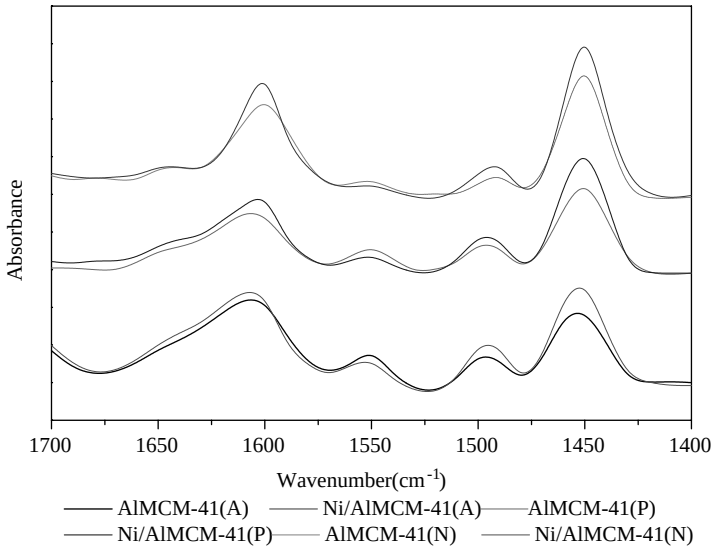

Figure 4. IR spectra of pyridine adsorbed on the samples after being degassed at 433 K.

Table 2
Acidity and Ni dispersion of the samples

Catalysts	Acidity[a] (mmol Py/g)			NH_3 desorbed[b] (mmol/g)	D_{Ni}[c](%)	n_{Ni}/n_A[d]
	B	L	*B* + *L*			
AlMCM-41(A)	0.54	0.78	1.32	0.55	–	
Ni/AlMCM-41(A)	0.52	0.88	1.40	0.63	11.1	0.07
AlMCM-41(P)	0.30	0.85	1.15	0.41	–	
Ni/AlMCM-41(P)	0.27	0.90	1.17	0.46	9.2	0.12
AlMCM-41(N)	0.20	0.91	1.11	0.26	–	
Ni/AlMCM-41(N)	0.19	0.95	1.14	0.31	8.9	0.16

[a] Calculated using the extinction coefficients by Emeis [24].
[b] NH_3 desorbed beyond 373 K.
[c] Nickel dispersion.
[d] n_{Ni}/n_A is the ratio of exposed nickel atoms number to the Bronsted acid number.

molecules, the much higher acidity of AlMCM-41(A) further confirmed that the Si—OH—Al sites were preferentially located at or near the wall surface of the mesostructure prepared using $NaAlO_2$ precursor as reported by Occelli [23]. After nickel impregnation, the Bronsted acid sites decreased while the Lewis acid sites largely increased. But the ultimate result was the increase of the total acid sites (Bronsted and Lewis acid sites), which was in good agreement with the NH_3-TPD (see table 2 and figure 3). The nickel modification over the acidity of the support had two different effects [20–22]. On the one hand, the Ni species could cover some acid sites (both Bronsted and Lewis acid sites), causing the decrease of the total acid sites. On the other hand, the coordinately unsaturated nickel cations could serve as a kind of new Lewis acid centers, which compensated the original covered Lewis acid sites. In the present case, the compensating effects of the Ni species override the covering ones that cause the increase of the total acid sites.

3.3. Surface metal function

All the catalysts exhibited two reduction stages (see figure 5), similarly to that reported elsewhere [25]. The low temperature reduction stage coincided with the reduction of Ni-oxide (most free nickel oxide with a bulk character), whereas the second reduction stage originated from the reduction of the small nickel oxide species, chemically bounded with the AlMCM-41 framework. For the Ni/AlMCM-41(A) catalyst, the low temperature peak was very small, shouldered with the broad high temperature peak maxim at 847 K, indicating that the Ni/AlMCM-41(A) catalyst mainly contained small nickel oxide particles, which had strong interaction with the support. By contrast, the Ni/

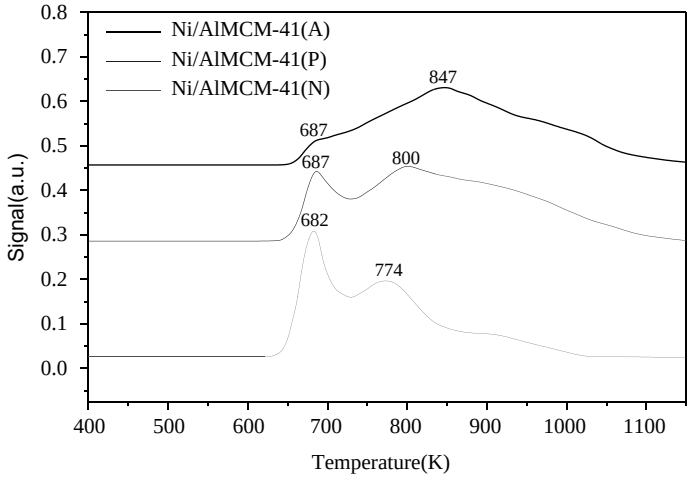

Figure 5. H_2-TPR profiles of the catalysts.

AlMCM-41(P) and Ni/AlMCM-41(N) catalysts demonstrated an intense low temperature peak and the high temperature reduction peak shifted to the lower temperature (maxim at 800 and 774 K, respectively), suggesting that there were more large NiO particles on the surface of the Ni/AlMCM-41(P) and Ni/AlMCM-41(N) catalysts and the nickel-support interaction was weaker than that of Ni/AlMCM-41(A) catalyst.

The nickel dispersion of the Ni/AlMCM-41 catalysts determined by hydrogen chemisorption was presented in table 2. The nickel dispersion of Ni/AlMCM-41(A) was higher than that of Ni/AlMCM-41(P) and Ni/AlMCM-41(N). Combined with the textural properties of the catalysts, the higher nickel dispersion of the nickel species in the case of Ni/AlMCM-41(A) catalyst might be ascribed to its higher surface area. Besides, the effective incorporation of Al atoms in the AlMCM-41 also improved the dispersion of Ni species as revealed by Klimova *et al*. [17].

3.4. Catalytic performance

The activities of the catalysts for *n*-dodecane hydroconversion versus temperature were shown in figure 6. At low reaction temperature, the total *n*-dodecane conversions were almost same. With the increase of temperature, the *n*-dodecane conversion over Ni/AlMCM-41(N) and Ni/AlMCM-41(P) increased faster than that over Ni/AlMCM-41(A), which ultimately caused the largely enhanced *n*-dodecane conversions over the former catalysts at higher temperature. Li *et al*. have reported that the *n*-dodecane conversion increased with the rise of the acid number over Pt/AlSBA-15 catalysts [26]. However, the behavior over the present Ni/AlMCM-41 catalysts could not positively correlate with the discrepancy of the acid number on the surface of the catalysts because the amount of the acid site in the order of Ni/AlMCM-41(N) < Ni/AlMCM-41(P) < Ni/AlMCM-41(A), which was contrary to the changing sequence of *n*-dodecane hydroconversion. The increasing hydrogenolysis reaction on the nickel sites (see figure 7), sharing a part of *n*-dodecane conversion on the Ni/AlMCM-41(N) and Ni/AlMCM-41(P) catalysts, might contribute to such behavior of *n*-dodecane hydroconversion.

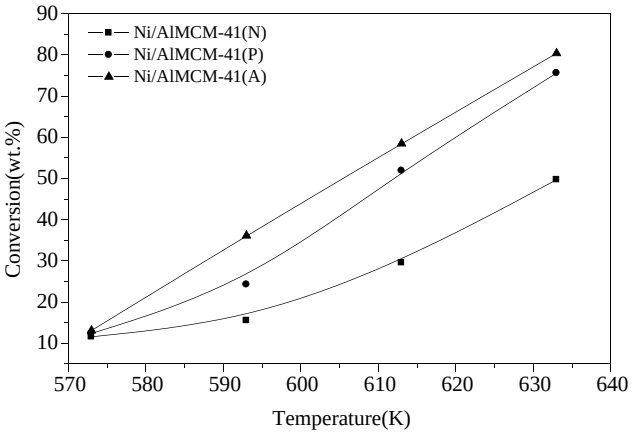

Figure 6. *n*-dodecane conversion as a function of temperature over Ni-supported catalysts.

The reaction pathways with respect to the hydrocracking, hydroisomerization and hydrogenolysis were depicted in figure 7. For the Ni/AlMCM-41(A) catalyst, the selectivity to the hydrocracking products increased monotonously at the expense of the decline of C_{12} isomers as the conversion increased. Meanwhile, little hydrogenolysis could be observed. The Ni/AlMCM-41(P) catalyst had the similar behavior to that of the Ni/AlMCM-41(A) catalyst, except that a noticeable hydrogenolysis products were produced at the higher *n*-dodecane conversion. For the Ni/AlMCM-41(N) catalyst, hydrogenolysis on metal sites was the most

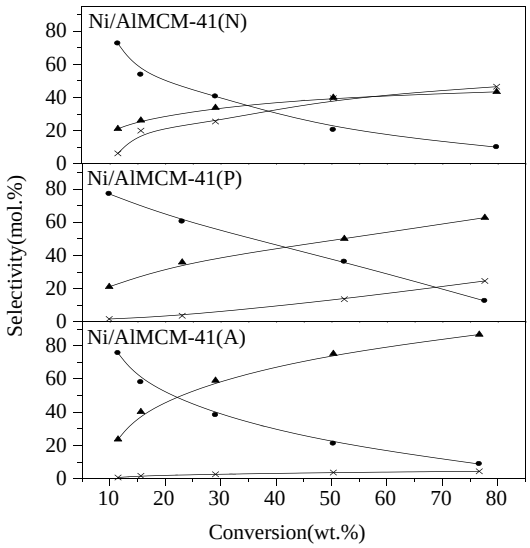

Figure 7. Different reaction selectivities of *n*-dodecane as a function of conversion. (●) Hydroisomerization; (▲) Hydrocracking; (×) Hydrogenolysis.

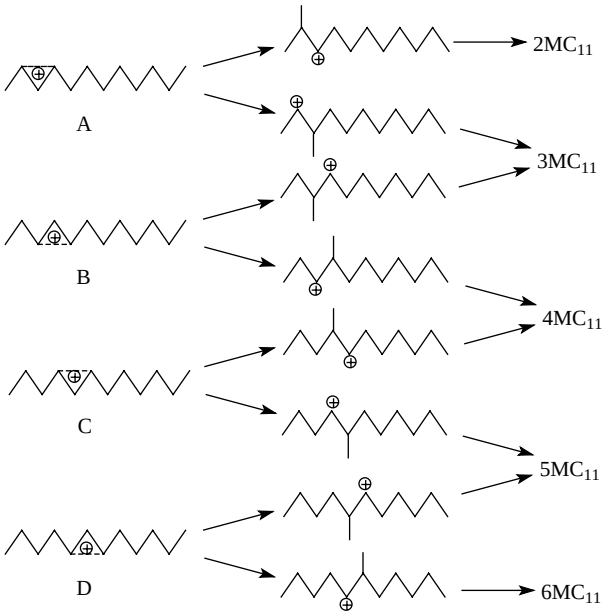

Scheme 1. Prediction of the methylundecane distribution from *n*-dodecane via protonated cyclopropane carbenium ions.

pronounced and even dominated over hydrocracking at higher conversion. The difference of the reaction pathway on the three catalysts was consistent with the characterization results of metal and acid functions. The acidity was strong to balance the metal function over Ni/AlMCM-41(A) catalyst, while the metal function dominated over the acid one on Ni/AlMCM-41(P) and Ni/AlMCM-41(N) catalysts. As a sequence, the hydrogenolysis reaction occurred on the nickel particles for the Ni/AlMCM-41(P) and Ni/AlMCM-41(N) catalysts but not for the Ni/AlMCM-41(A) catalyst.

The composition of monobranched C_{12} isomers at the similar conversion level was given in table 3. For all the catalysts, the distribution of methylundecane differed little. According to the proposed PCP mechanism [27], we could predict the following molar distribution of methylundecane (see scheme 1): $2MC_{11}$, 12.5%; $3MC_{11}$, 25%; $4MC_{11}$, 25%; $5MC_{11}$, 25%; $6MC_{11}$, 12.5%. Obviously, the experimental result deviated from the predicted one based on the proposed PCP mechanism. This implied that a fraction of methylundecane generated via protonated cyclopropane intermediates further proceeded the classical methyl shift process. Smirniotis *et al.* also reported the similar results when they investigated the *n*-octane hydroconversion over a series of Pt/Zeolite catalysts [2]. Therefore, both studies demonstrated that the alkyl shift and PCP branching were occurred simultaneously in the *n*-paraffin isomerization. The ratio of monobranched to multibranched dodecane isomers (M/B) declined with the increase of conversion due to the degree of branching increased at higher conversion (see figure 8). In addition, the M/B ratio was higher over Ni/AlMCM-41(N) than that over Ni/AlMCM-41(A) and Ni/AlMCM-41(P) at given conversion, which might be ascribed to the severe hydrogenolysis on the Ni/AlMCM-41(N) catalyst.

Table 3
Molar Distribution of Monobranched C_{12} isomers

Catalyst	Ni/AlMCM-41(A)	Ni/AlMCM-41(P)	Ni/AlMCM-41(N)
$X_{n-C_{12}}$(%)	29.05	25.07	29.08
2 MC_{11}	19.07	18.52	18.96
3 MC_{11}	25.20	23.98	25.07
4 MC_{11}	20.68	21.26	21.22
(5 + 6)MC_{11}	35.05	36.24	34.74

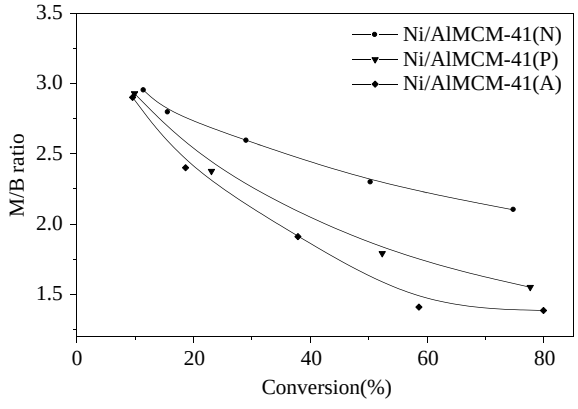

Figure 8. The ratio of monobranched to multibranched dodecane isomers (M/B) as a function of conversion.

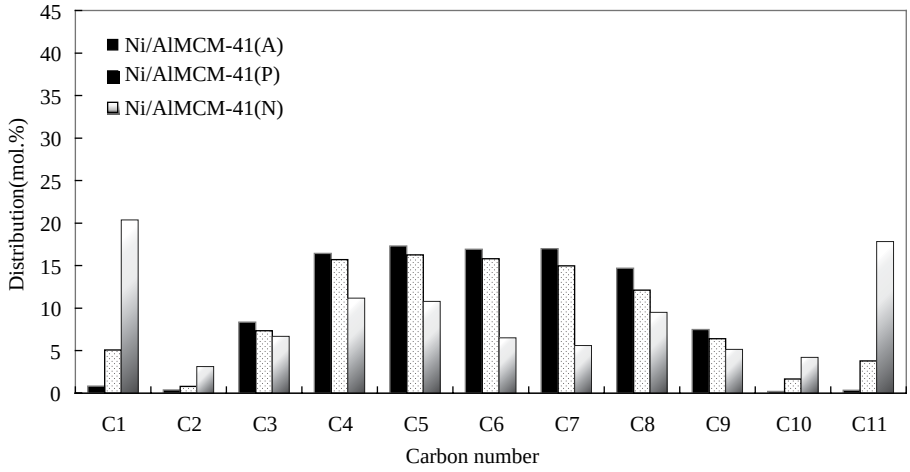

Figure 9. Distribution of the cracked products over the nickel-containing catalysts at the conversion of ca. 29%.

Table 4
Composition of some cracked products on the Ni-supported catalysts

Catalyst	$X_{n-C_{12}}$ (%)	C_3/C_1 (molar)	C_4–C_9 (mol%)	i/n (C_4–C_9) (molar)
Ni/AlMCM-41(A)	29.05	10.0	89.86	1.75
Ni/AlMCM-41(P)	25.07	1.45	81.27	1.18
Ni/AlMCM-41(N)	29.08	0.32	68.13	0.66

The carbon number distribution of cracked products at approximately conversion (ca. 29%) was presented in figure 9. The Ni/AlMCM-41(A) catalyst showed a nearly symmetrical distribution centered at C_6, while the Ni/AlMCM-41(P) and Ni/AlMCM-41(N) catalyst, especially the latter, gave lots of methane and undecane. In addition, the largest amount of C_4–C_9 hydrocarbons (mainly their isomers) could be obtained over Ni/AlMCM-41(A) catalyst (see table 4), which was also much more than that obtained over the reported Ni/HZSM-5 catalyst for *n*-dodecane hydroconversion [28]. These results indicated that the *n*-dodecane exhibited a primary cracking behavior over Ni/AlMCM-41(A) catalyst. For an ideal bifunctional catalyst, the carbon number distribution of the cracked products is symmetrical and the ratio of metal function to acidity (n_{Ni}/n_A) has an optimum value. When the n_{Ni}/n_A is higher than the optimum value, hydrogenolysis reaction will be predominant. On the contrary, the consecutive cracking reaction will prevail. Therefore, it could be considered that the Ni/AlMCM-41(A) was an ideal bifunctional catalyst for the *n*-dodecane hydroconversion and the n_{Ni}/n_A ratio of 0.07 (see table 2) was a proper value to guarantee the balance between metal and acid functions.

4. Conclusions

The mesoporous aluminosilicate (AlMCM-41) prepared with $NaAlO_2$ precursor contained more framework Al(IV) species and stronger acidity compared with the ones prepared with $Al(NO_3)_3$ and $Al(OPr^i)_3$. Supported with 2.0 wt% nickel metal, the Lewis acid sites of the AlMCM-41 samples increased due to the compensating effect of the coordinately unsaturated nickel cations, while the Bronsted acid sites slightly decreased because of the coverage of the nickel species. For *n*-dodecane hydroconversion, the Ni/AlMCM-41 catalyst prepared with $NaAlO_2$ gave the symmetrical carbon number distribution and a large amount of C_4—C_9 hydrocarbons in the cracked products due to its proper balance between metal and acid functions.

Acknowledgments

The authors gratefully acknowledge the funding of this project by National Key Fundamental Research and Development Projects of China (Project ID G1999022402).

References

[1] A. Lugstein, A. Jentys and H. Vinek, Appl. Catal. A 152 (1997) 93.
[2] W. Zhang and P.G. Smirniotis, J. Catal. 182 (1999) 400.
[3] M.D. Romero, A. de Lucas, J.A. Calles and A. Rodriguez, Appl. Catal. A 146 (1996) 425.
[4] S.T. Sie, Ind. Eng. Chem. Res. 32 (1993) 403.
[5] J.A. Martens and P.A. Jacobs, *Theoretical Aspects of Heterogeneous Catalysis*, Van Nostrand Reinhold, New York, 1990.
[6] A. Lugstein, A. Jentys and H. Vinek, Appl. Catal. 176 (1999) 119.
[7] W.J.J. Welters, O.H. van der Waerden, V.H.J. de Beer and R.A. van Santen, Ind. Eng. Chem. Res. 34 (1995) 1166.
[8] D. Li, F. Li, J. Ren and Y. Sun, 241 (2003) 15.
[9] A. Corma, A. Martinez, S. Pergher, S. Peratello, C. Perego and G. Bellusi, Appl. Catal. A 152 (1997) 107.
[10] K.M. Reddy and C. Song, Catal. Today 31 (1996) 137.
[11] S.P. Elangovan, C. Bischof and M. Hartmann, Catal. Lett. 80 (1–2) (2002) 35.
[12] K.J. Del Rossi, G.H. Hatzikos and A. Huss, US Patent 5, 256, 277 assigned to Mobil Oil Corp, 1993.

[13] K. Chaudhari, T.K. Das, A.J. Chandwadkar and S. Sivasanker, J. Catal. 186 (1999) 81.
[14] A. Klemt, A. Taouli, H. Koch and W. Reschetilowski, Stud. Surf. Sci. Catal. 127 (1999) 405.
[15] R. Mokaya and W. Jones. Chem. Commun. (1997) 2185.
[16] Y.H. Yue, Y. Sun, Q. Xu and Z. Gao, Appl. Catal. 175 (1998) 131.
[17] T. Klimova, M. Calderon and J. Ramirez, Appl. Catal. A 6225 (2002) 1.
[18] A. Lewandowska, S. Monteverdi, M. Bettahar and M. Ziolek, J. Mol. Catal. A Chemical 188 (2002) 85.
[19] A. Jentys, N.H. Pham and H. Vinek, J. Chem. Soc. Farday Trans. 92 (1996) 3287.
[20] Yamagishik, I. Nakamura, S. Nakai and A. Iino, in: *Proceeding of 9th IZC Montreal*, Canada, 1992, RP68.
[21] C. Minchev, S.A. Zubkov, V. Valtchev and V. Minkov, Appl. Catal. A 119 (1994) 195.
[22] M.D. Romero, J.A. Calles and A. Rodriguez, Ind. Eng. Chem. Res. 36 (1997) 3533.
[23] M.L. Occelli, S. Biz, A. Auroux and G.J. Ray, Micropor. Mesopor. Mater. 26 (1998) 193.
[24] C.A. Emeis, J. Catal. 141 (1993) 347.
[25] D.J. Lensveld, J.G. Mesu, A. Jos van Dillen and K.P. de Jong, Micropor. Mesopor. Mater. 44–45 (2001) 401.
[26] C. Nie, L. Huang, D. Zhao and Q. Li, Catal. Lett. 71 (1–2) (2001) 117.
[27] J.A. Martens and P.A. Jacobs, Zeolites 6 (1986) 334.
[28] A. Arcoya and X.L. Seoane, React. Kinet. Catal. Lett. 41 (1) (1990) 181.